Article ID: 1000-324X(2021)11-1217-06 **DOI:** 10.15541/jim20200744

$CsPbBr_3$ Perovskite Quantum Dots/Ultrathin C_3N_4 Nanosheet 0D/2D Composite: Enhanced Stability and Photocatalytic Activity

SHU Mengyang, LU Jialin, ZHANG Zhijie, SHEN Tao, XU Jiayue

(School of Materials Science and Engineering, Shanghai Institute of Technology, Shanghai 201418, China)

Abstract: Metal-halide perovskite quantum dots (QDs) have emerged as a potential photocatalyst owing to their remarkable optoelectronic properties. However, the poor stability and insufficient charge transportation efficiency of this type of materials hindered their applications in the photocatalysis field. Herein, we decorated $CsPbBr_3$ QDs on two-dimensional (2D) ultrathin g-C_3N_4 (UCN) nanosheets to develop a 0D/2D $CsPbBr_3$/UCN composite photocatalyst. The introduction of UCN can not only improve the stability of $CsPbBr_3$ QDs by passivating the surface ligands of $CsPbBr_3$ QDs, but also facilitate the charge transfer due to the suited band gap alignment. Consequently, the obtained $CsPbBr_3$/UCN heterostructure exhibited superior photocatalytic performance to both pristine $CsPbBr_3$ QDs and UCN. This work has provided an efficient strategy for the design of $CsPbX_3$-based heterostructure with high stability and photocatalytic activity.

Key words: perovskite quantum dots; 2D ultrathin nanosheets; photocatalysis; $CsPbBr_3$; g-C_3N_4

In the past few years, metal-halide perovskite quantum dots (QDs) have attracted enormous attention for its remarkable optoelectronic properties, such as excellent absorption ability, high-quantum-yield photoluminescence, tunable band gap, long carrier lifetime and so on[1-4]. The outstanding advantages of these materials have triggered great interest for optoelectronic and photovoltaic applications, such as light-emitting diode devices, photodetectors, displays and solar cells[5-9]. More recently, the metal-halide perovskite QDs ($CsPbBr_3$) was found to be a promising photocatalyst owing to its outstanding optical features with the combined advantages of wide spectral absorption scope and suitable bandgap[10-11]. Despite of all these advantages, the inherent poor stability of metal-halide perovskite QDs has always been the obstacle to restricting these materials for photocatalytic applications, especially in aqueous solution. If the instability issues of these materials can be addressed, metal-halide perovskite QDs are expected to be strong candidates for photocatalytic applications on considering their remarkable optical properties.

Recently, two-dimensional (2D) materials have aroused extensive attention from researchers due to their exceptional electronic and optical properties compared with their bulk counterparts[12-14]. According to the previous studies, metal-halide perovskite QDs can be passivated by anchoring them on some two dimensional materials (*e.g.*, Graphitic carbon nitride (g-C_3N_4) and graphene oxide)[10,15], to prevent the crystal structure of the perovskite QDs from decomposition. Especially, 2D g-C_3N_4 nanosheets have gained special attractions owing to its suitable bandgap, high chemical stability, abundance and low cost, which makes it a potential candidate for solar energy conversion, environment purification, and bioimaging applications[16-21]. In view of the above advantages, g-C_3N_4 can be served as an ideal material to passivate perovskite QDs. Besides stability enhancement, the combination of $CsPbBr_3$ and g-C_3N_4 can bring about another benefit: the energy band structure between $CsPbBr_3$ and g-C_3N_4 is a type II band alignment, which can facilitate the charge carrier transfer between the two components[22]. Zhao *et al.*[22]have coupled $CsPbBr_3$ QDs with bulk g-C_3N_4 and demonstrated its enhanced photocatalytic degradation activity for penicillins 6-APA. You *et al.* [23] have also combined $CsPbBr_3$ QDs with bulk g-C_3N_4 to fabricate a $CsPbBr_3$@g-C_3N_4 composite, which showed enhanced photocatalytic activity in CO_2 reduction. The above research results suggested that the

Received date: 2020-12-30; **Revised date:** 2021-04-01; **Published online:** 2021-05-10
Foundation item: National Natural Science Foundation of China (51972213)
Biography: SHU Mengyang(1996-), male, Master candidate. E-mail: 277550283@qq.com
舒孟洋(1996–), 男, 硕士研究生. E-mail: 277550283@qq.com
Corresponding author: ZHANG Zhijie, associate professor. E-mail: zjzhang@sit.edu.cn; XU Jiayue, professor. E-mail: xujiayue@sit.edu.cn
张志洁, 副教授. E-mail: zjzhang@sit.edu.cn; 徐家跃, 教授. E-mail: xujiayue@sit.edu.cn

construction of $CsPbBr_3$/g-C_3N_4 heterostructure can be an efficient strategy to develop an ideal photocatalyst with desirable stability and photocatalytic activity.

In this contribution, ultrathin g-C_3N_4 (UCN) nanosheets were employed to combine with $CsPbBr_3$ QDs, with the aim of coupling 2D ultrathin g-C_3N_4 nanosheets with 0D $CsPbBr_3$ QDs to obtain a 0D/2D composite photocatalyst with high performance. The photocatalytic performance of the obtained 0D/2D $CsPbBr_3$/UCN composite was evaluated by the degradation of a typical pollutant in water, Rhodamine B (RhB). Benefitting from the suitable energy band structure, such a 0D/2D heterostructure exhibited enhanced photocatalytic activity than both pristine $CsPbBr_3$ QDs and UCN. Furthermore, due to the strong interaction between $CsPbBr_3$ QDs and UCN, the stability of $CsPbBr_3$ QDs was greatly enhanced.

1 Experimental

1.1 Material preparation

1.1.1 Preparation of ultrathin g-C_3N_4 nanosheets

Bulk g-C_3N_4 was first prepared by pyrolysis of melamine at 550 ℃ for 4 h with a ramp rate of 2.5 ℃/min, which was donated as BCN. Ultrathin g-C_3N_4 nanosheets were synthesized by exfoliating BCN as follows: 320 mg of BCN was mixed with 6 mol/L HCl solution (80 mL), which was then transferred into a 100 mL Teflonlined autoclave and heated at 110 ℃ for 5 h. Upon cooling, the precipitate was filtered, washed and dried at 80 ℃ under vacuum for 12 h. The obtained ultrathin g-C_3N_4 nanosheets was donated as UCN.

1.1.2 Preparation of $CsPbBr_3$ QDs

$CsPbBr_3$ QDs was synthesized using a typical hot-injection method published by Protesescu *et al*[24]. Firstly, the Cs-oleate solution was prepared by adding 0.817 g Cs_2CO_3, 3 mL oleic acid, and 30 mL octadecene into a three-neck flask under Ar atmosphere, which was heated to 130 ℃ until all Cs_2CO_3 was dissolved. Then 0.132 g $PbBr_2$, 10 mL octadecene, 1 mL oleic acid, and 1 mL oleylamine were loaded into another three-neck flask, which was dried at 130 ℃ under Ar atmosphere. After the complete dissolution of $PbBr_2$, the temperature was increased to 160 ℃, and 1 mL Cs-oleate precursor was quickly injected. 5 s later, the reaction was terminated by ice water. The final product was obtained by centrifugation, washing and drying at 60 ℃ under vacuum for 12 h.

1.1.3 Preparation of $CsPbBr_3$/UCN composite

The preparation process of the $CsPbBr_3$/UCN composite was illustrated in Scheme 1: 10 mg of the obtained $CsPbBr_3$ QDs was dispersed in 10 mL toluene, then 90 mg of the as-prepared UCN was added into the $CsPbBr_3$ QDs ink solution. After stirring for several hours, the color of ink solution turned from yellow to colorless, indicating that $CsPbBr_3$ QDs have anchored on UCN. The precipitate was centrifuged to obtain the $CsPbBr_3$/UCN composite.

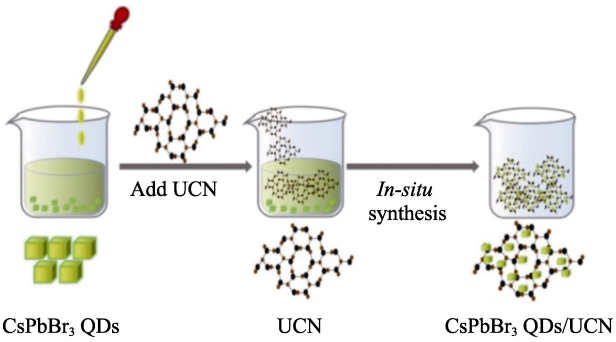

Scheme 1 Illustration of the preparation process of $CsPbBr_3$/UCN composite.

1.2 Characterization

The phase identification of the as-prepared products were characterized by X-ray diffraction (XRD, D/max 2200PC) using Cu Kα radiation. The morphologies of the products were observed by transmission electron microscope (TEM, FEI tecnaiG2F30) operated at 200 kV. The optical absorption spectra of the products were obtained from a PE Lambda 900 UV-visible spectrophotometer. The carrier separation ability of the samples were characterized by Photoluminescence (PL) spectra on a fluorescence spectrometer (FluoroMax-4) and photo-electrochemical experiments on an electrochemical system (CHI-650E) with three-electrode system.

1.3 Photocatalytic experiments

Photocatalytic experiments were carried out under a 500 W Xe lamp with 420 nm UV filter. In a typical procedure, 50 mg of as-prepared photocatalyst and 50 mL of RhB solution (10^{-5} mol/L) were mixed in a beaker. After being stirred in the dark for 60 min, the mixture was illuminated under visible light and 3 mL of the suspension was withdrawn at given intervals. After the photocatalyst particles being removed by centrifugation, the absorption spectral change of the supernatant was measured with a PE Lambda 900 UV-Vis spectrophotometer. The concentration change of RhB was obtained by monitoring the absorption band maximum at 552 nm.

2 Results and discussion

2.1 Crystal structure

The crystal structures of $CsPbBr_3$ QDs, UCN and $CsPbBr_3$/UCN composite were characterized by XRD patterns. As exhibited in Fig. 1, the peaks of the as-prepared $CsPbBr_3$ QDs matched well with the orthorhombic $CsPbBr_3$ (JCPDS 18-0364). For the UCN sample, two diffraction

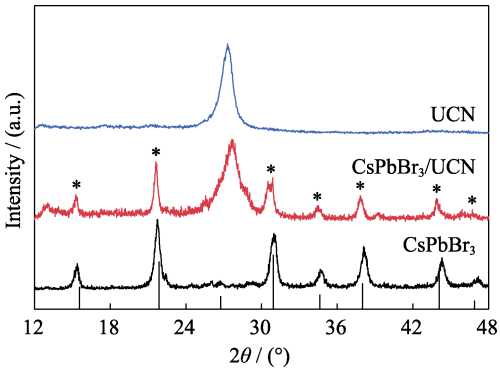

Fig. 1　XRD patterns of $CsPbBr_3$, UCN and $CsPbBr_3$/UCN composite

peaks at 2θ=13.2° and 27.7° can be observed, corresponding to the (100) and (002) diffraction planes of g-C_3N_4, respectively[25]. The characteristic diffraction peaks of both $CsPbBr_3$ QDs and g-C_3N_4 could be observed in the XRD pattern of the $CsPbBr_3$/UCN composite, suggesting the successful loading of $CsPbBr_3$ QDs on UCN.

2.2　Morphology analysis

TEM was employed to investigate the morphology of the as-fabricated $CsPbBr_3$ QDs, UCN and $CsPbBr_3$/UCN composite. Fig. 2(A) shows the TEM image of $CsPbBr_3$ QDs, demonstrating a cubic-shaped morphology with fairy uniform size of around 10 nm. As shown in Fig. 2(B), the UCN sample is composed of thin nanosheets, indicating the successful exfoliation of bulk g-C_3N_4. In the TEM image of $CsPbBr_3$/UCN composite (Fig. 2(C)), it can be seen that $CsPbBr_3$ QDs are dispersed on UCN nanosheets. Moreover, a clear lattice spacing of 0.58 nm is observed from the HRTEM image of the $CsPbBr_3$ QDs on UCN (Fig. 2(D)), which is attributed to the (100) plane of orthorhombic $CsPbBr_3$[26].

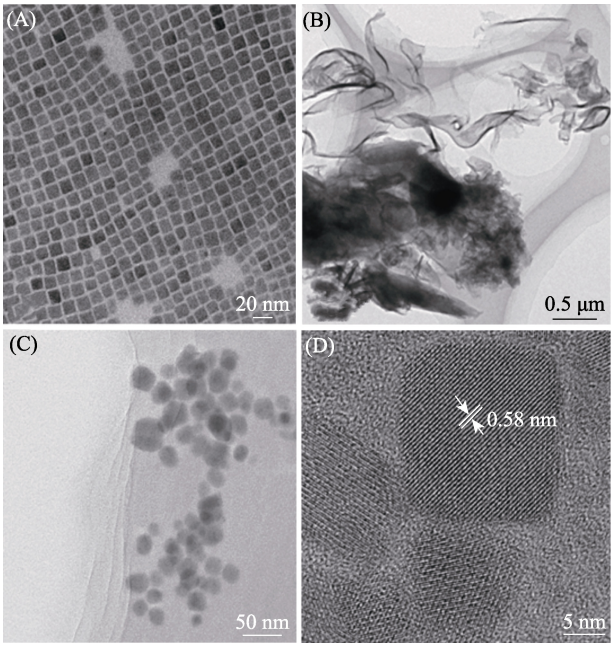

Fig. 2　TEM image of (A) $CsPbBr_3$ QDs, (B) UCN and (C) $CsPbBr_3$/UCN composite; (D) HRTEM image of $CsPbBr_3$/UCN composite

2.3　Optical properties

The optical properties of $CsPbBr_3$ QDs, UCN and $CsPbBr_3$/UCN composite were investigated by UV-Vis diffused absorption spectra, which were exhibited in Fig. 3. UCN displayed a visible absorption edge at 473 nm, which corresponded to a bandgap energy of 2.62 eV. $CsPbBr_3$ QDs showed the absorption edge at around 550 nm, illustration of a bandgap energy of 2.25 eV. Compared to the pure $CsPbBr_3$ QDs and pure UCN, a notable red-shift of the absorbance and enhanced light-harvesting of the $CsPbBr_3$/UCN composite is observed, which can be ascribed to the synergistic effect of $CsPbBr_3$ QDs and UCN, implying a more efficient utilization of visible light during the photocatalytic reaction.

2.4　Evalution of photocatalytic activity

In order to assess the practicability of the $CsPbBr_3$/UCN composite in the photocatalytic applications, the degradation of RhB was performed. As shown in Fig. 4(A), the $CsPbBr_3$/UCN composite exhibited noticeably improved photocatalytic activity than pure $CsPbBr_3$ QDs and pure UCN, which can almost completely degrade RhB after 15 min visible light irradiation, accompanied with a total organic carbon (TOC) removal efficiency of 82.6%. The high degree of mineralization of organic species confirms that RhB has been photocatalytically decomposed. Moreover, to assess the superiority of UCN, the photocatalytic activity of bulk g-C_3N_4 (BCN) was also evaluated, which was much lower than that of UCN and $CsPbBr_3$/UCN composite. In addition, the stability of the photocatalyst is an important factor limiting its practical application. As is known, $CsPbBr_3$ QDs have poor water stability, since they are subjected to structural decomposition in aqueous phase[27]. To assess the stability of the photocatalyst, the powders are recovered after the photocatalytic experiments and characterized by XRD.

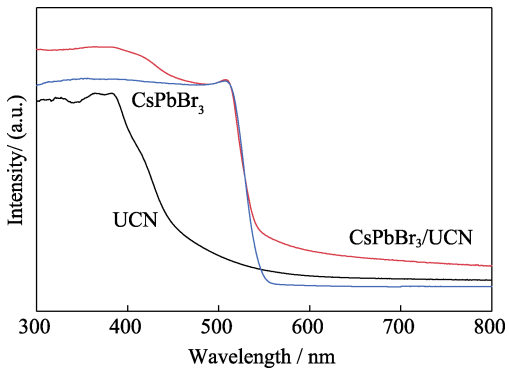

Fig. 3　UV-Vis diffuse reflectance spectra of $CsPbBr_3$, UCN and $CsPbBr_3$/UCN composite

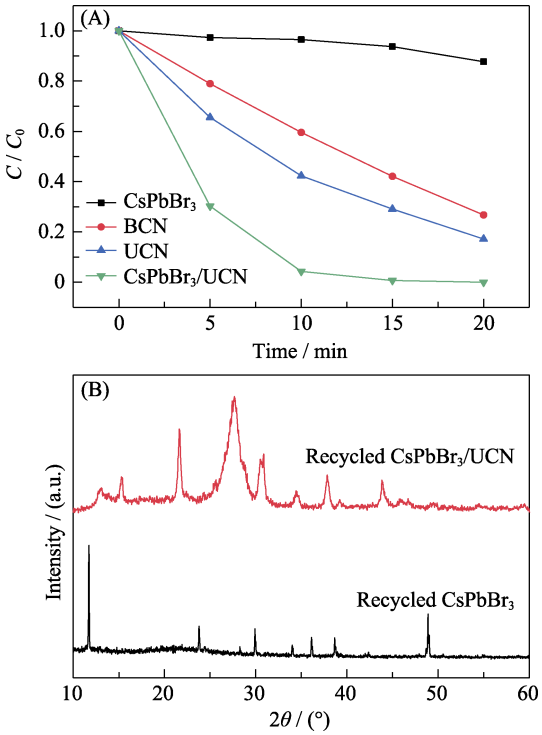

Fig. 4 (A) Photocatalytic degradation of RhB over $CsPbBr_3$, BCN, UCN and $CsPbBr_3$/UCN composite; (B) XRD patterns of recycled $CsPbBr_3$ and $CsPbBr_3$/UCN composite

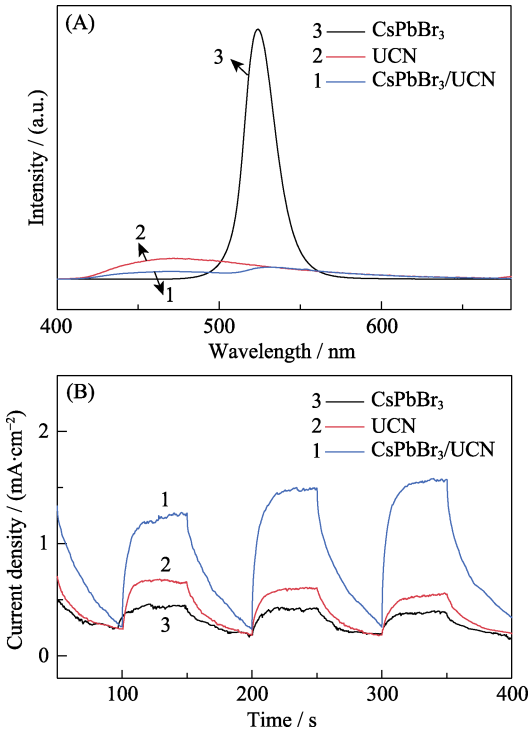

Fig. 5 (A) PL spectra and (B) transient photocurrent responses of $CsPbBr_3$, UCN and $CsPbBr_3$/UCN composite

As shown in Fig. 4(B), severe structure degradation is observed for the $CsPbBr_3$ QDs after water immersion, while the crystal structure of the $CsPbBr_3$/UCN composite is well preserved, demonstrating the good water stability of the $CsPbBr_3$/UCN composite. The stability enhancement could be ascribed to the formation of N–Br bonding between $CsPbBr_3$ QDs and UCN. Since amino group can interact strongly with $CsPbBr_3$ QDs through the surface bromide, the resultant $CsPbBr_3$/UCN composite is more stable than organic ligands passivation.

2.5 Photocatalytic mechanism

For an ideal photocatalyst, the expanded spectral response scope, and the effective charge separation and transportation ability are desired. As shown in Fig. 3, the spectral response scope of the $CsPbBr_3$/UCN composite were obviously extended compared with pure $CsPbBr_3$ and UCN, indicating more light-harvesting of the $CsPbBr_3$/UCN composite. In order to investigate the photon-generated charge separation and migration abilities of the as-prepared products, PL spectra and transient photocurrent response experiments were performed. As shown in Fig. 5(A), $CsPbBr_3$ QDs exhibited a strong emission peak at 520 nm, while anchoring $CsPbBr_3$ on the UCN drastically reduced the PL intensity. Besides, the emission intensity originated from UCN also decreased slightly, implying the occurrence of photo-generated carrier transfer between $CsPbBr_3$ and UCN. Moreover, the transient photocurrent response spectra (Fig. 5(B)) showed that the $CsPbBr_3$/UCN composite exhibited significantly higher photocurrent response intensities than both $CsPbBr_3$ QDs and UCN, which indicated more efficient charge transfer of the $CsPbBr_3$/UCN composite.

Mott-Schottky measurements were performed to determine the band potentials of UCN and $CsPbBr_3$. As shown in Fig. 6(A), both UCN and $CsPbBr_3$ feature a typical n-type semiconductor, with the flat band potential values of –1.01 and –0.91 eV *versus* the saturated calomel electrode (SCE), respectively. Correspondingly, the valance band positions for UCN and $CsPbBr_3$ are 1.61 and 1.14 eV (*vs.* NHE) based on the calculated bandgap, respectively. Hence, the band alignments of both samples are illustrated in Fig. 6(B). It is clear that the conduction band minimum (CBM) of UCN is lower than that of $CsPbBr_3$, and the valence band maximum (VBM) of UCN is lower than that of $CsPbBr_3$. Therefore, the conduction band electrons of $CsPbBr_3$ can transfer to that of UCN, while the valence band holes of UCN can migrate to that of $CsPbBr_3$. As such, effective charge separation and inhibition of charge recombination in the composite photocatalyst is realized, which led to the improved photocatalytic activity.

3 Conclusions

In summary, we have successfully fabricated a $CsPbBr_3$/UCN composite *via* a facile process, which can be used as an efficient and stable photocatalyst in water

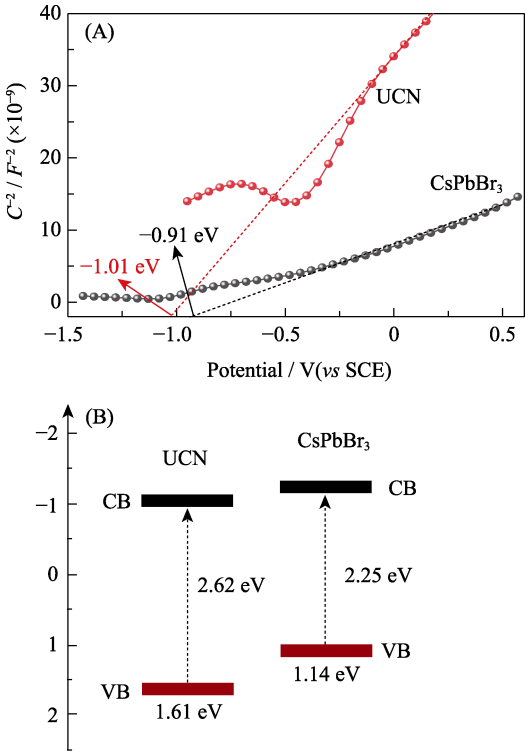

Fig. 6　(A) Electrochemical Mott-Schottky plots and (B) band alignments of $CsPbBr_3$ and UCN

medium. Microstructure characterization showed that the $CsPbBr_3$ QDs were anchored on the surface of UCN to form a 0D/2D heterostructure. The formation of the $CsPbBr_3$/UCN heterostructure can greatly facilitate photo-generated charge separation and transportation, as disclosed by the PL spectra and the photoelectrochemical measurements. The expanded light-harvesting scope, as well as the enhanced charge separation efficiency are responsible for the improved photocatalytic activity of the $CsPbBr_3$/UCN composite. This work may provide a useful guide towards the utilization of metal halide perovskite for photocatalytic applications.

References:

[1] LI H T, HE X D, LIU Y, *et al.* One-step ultrasonic synthesis of water-soluble carbon nanoparticles with excellent photoluminescent properties. *Carbon*, 2011, **49(2):** 605–609.

[2] GAO Y, ZHAO L, SHANG Q, *et al.* Ultrathin $CsPbX_3$ nanowire arrays with strong emission anisotropy. *Advanced Materials*, 2018, **30(31):** 1801805.

[3] LI J, XU L, WANG T, *et al.* 50-fold EQE improvement up to 6.27% of solution-processed all-inorganic perovskite $CsPbBr_3$ QLEDs *via* surface ligand density control. *Advanced Materials*, 2017, **29(5):** 1603885.

[4] WANG H R, ZHANG X Y, WU Q Q, *et al.* Trifluoroacetate induced small-grained trifluoroacetate induced small-grained stable light-emitting devices. *Nature Communications*, 2019, **10(1):** 665.

[5] DING J, DU S, ZUO Z, *et al.* High detectivity and rapid response in perovskite $CsPbBr_3$ single-crystal photodetector. *Journal of Physical Chemistry C*, 2017, **121(9):** 4917–4923.

[6] BEGUM R, PARIDA M R, ABDELHADY A L, *et al.* Engineering interfacial charge transfer in $CsPbBr_3$ perovskite nanocrystals by heterovalent doping. *Journal of the American Chemical Society*, 2017, **139(2):** 731–737.

[7] LAO X Z, YANG Z, SU Z C, *et al.* Luminescence and thermal behaviors of free and trapped excitons in cesium lead halide perovskite nanosheets. *Nanoscale*, 2018, **10(21):** 9949–9956.

[8] LEE Y H, LUO J, BAKER R H, *et al.* Unraveling the reasons for efficiency loss in perovskite solar cells. *Advanced Functional Materials*, 2015, **25(25):** 3925–3933.

[9] TAN Y S, LI R Y, XU H, *et al.* Ultrastable and reversible fluorescent perovskite films used for flexible instantaneous display. *Advanced Functional Materials*, 2019, **29(23):** 1900730.

[10] XU Y F, YANG M Z, CHEN B X, *et al.* A $CsPbBr_3$ perovskite quantum dot/graphene oxide composite for photocatalytic CO_2 reduction. *Journal of the American Chemical Society*, 2017, **139(16):** 5660−5663.

[11] WU Y Q, WANG P, ZHU X L, *et al.* Composite of $CH_3NH_3PbI_3$ with reduced graphene oxide as a highly efficient and stable visible-light photocatalyst for hydrogen evolution in aqueous HI solution. *Advanced Materials*, 2018, **30(7):** 1704342.

[12] FENG J, PENG L L, WU C Z, *et al.* Giant moisture responsiveness of VS_2 ultrathin nanosheets for novel touchless positioning interface. *Advanced Materials*, 2012, **24(15):** 1969−1974.

[13] LOH K P, BAO Q L, EDA G, *et al.* Graphene oxide as a chemically tunable platform for optical applications. *Nature Chemistry*, 2010, **2(12):** 1015−1024.

[14] ZHANG X D, XIE X, WANG H, *et al.* Enhanced photoresponsive ultrathin graphitic-phase C_3N_4 nanosheets for bioimaging. *Journal of the American Chemical Society*, 2013, **135(1):** 18−21.

[15] OU M, TU W G, YIN S G, *et al.* Amino-assisted anchoring of $CsPbBr_3$ perovskite quantum dots on porous g-C_3N_4 for enhanced photocatalytic CO_2 reduction. *Angewandte Chemie International Edition*, 2018, **130(41):** 13758–13762.

[16] WANG X C, BLECHERT S, ANTONIETTI M, *et al.* Polymeric graphitic carbon nitride for heterogeneous photocatalysis. *ACS Catalysis*, 2012, **2(8):** 1596−1606.

[17] CAO S W, YU J G. g-C_3N_4 based photocatalysts for hydrogen production. *Journal of Physical Chemistry Letters*, 2014, **5(12):** 2101−2107.

[18] LIU Q, CHEN T X, GUO Y R, *et al.* Ultrathin g-C_3N_4 nanosheets coupled with carbon nanodots as 2D/0D composites for efficient photocatalytic H_2 evolution. *Applied Catalysis B: Environmental*, 2016, **193(15):** 248–258.

[19] ZHU M S, KIN S, MAO L, *et al.* Metal-free hotocatalyst for H_2 evolution in visible to near-infrared region: black phosphorus/graphitic carbon nitride. *Journal of the American Chemical Society*, 2017, **139(37):** 13234–13242.

[20] ZHAO Y Y, LIANG X H, WANG Y B, *et al.* Degradation and removal of ceftriaxone sodium in aquatic environment with Bi_2WO_6/g-C_3N_4 photocatalyst. *Journal of Colloid and Interface Science*, 2018, **523(1):** 7–17.

[21] HUANG H R, ZHANG Z Z, GUO S K, *et al.* Interfacial charge-transfer transitions enhanced photocatalytic activity of TCNAQ/g-C_3N_4 organic hybrid material. *Materials Letters*, 2019, **255(15):** 126546.

[22] ZHAO Y Y, SHI H X, HU X Y, *et al.* Fabricating $CsPbX_3$/CN hetero-structures with enhanced photocatalytic activity for penicillins 6-APA degradation. *Chemical Engineering Journal*, 2020, **381(1):** 122692.

[23] YOU S Q, GUO S H, ZHAO X, *et al.* All-inorganic perovskite/graphitic carbon nitride composite for CO_2 photoreduction into C1 compounds under low concentrations of CO_2. *Dalton Transactions*, 2019, **48(37):** 14115–14121.

[24] PROTESESCU L, YAKUNIN S, BODNARCHUK M I, *et al.* Nanocrystals of cesium lead halide perovskites ($CsPbX_3$, X=Cl, Br, and I): novel optoelectronic materials showing bright emission with wide color gamut. *Nano Letters*, 2015, **15(6):** 3692−3696.

[25] ZOU Y, YANG B, LIU Y, *et al.* Controllable interface-induced co-assembly toward highly ordered mesoporous Pt@TiO_2/g-C_3N_4 heterojunctions with enhanced photocatalytic performance. *Advanced Functional Materials*, 2018, **28(50):** 1806214.

[26] LIANG Z Q, ZHAO S L, XU Z, *et al.* Shape-controlled synthesis of all-inorganic $CsPbBr_3$ perovskite nanocrystals with bright blue emission. *ACS Applied Materials Interfaces*, 2016, **8(42):** 28824–28830.

[27] PARK S, CHANG W J, LEE C W, *et al.* Photocatalytic hydrogen generation from hydriodic acid using methylammonium lead iodide in dynamic equilibrium with aqueous solution. *Nature Energy*, 2016, **2(1):** 16185.

$CsPbBr_3$ 钙钛矿量子点/C_3N_4 超薄纳米片 0D/2D 复合材料: 增强的稳定性和光催化活性

舒孟洋, 陆嘉琳, 张志洁, 沈 涛, 徐家跃

(上海应用技术大学 材料科学与工程学院, 上海 201418)

摘 要: 金属卤化物钙钛矿量子点(QDs)具有良好的光电性质, 是一种潜在的光催化剂材料。但是, 它的稳定性较差, 并且电荷传输效率不足, 阻碍了其在光催化领域的应用。本工作将 $CsPbBr_3$ 量子点装饰在二维超薄 g-C_3N_4 纳米片(UCN)上, 制备了 0D/2D $CsPbBr_3$/UCN 复合光催化剂。引入 UCN 不仅可以通过钝化 $CsPbBr_3$ 量子点的表面配体来提高 $CsPbBr_3$ 量子点的稳定性, 而且两者的能带匹配还可以促进两种材料之间的电荷转移。 因此, 所制备的 $CsPbBr_3$/UCN 异质结构比单纯的 $CsPbBr_3$ 量子点和 UCN 具有更优越的光催化性能, 这为设计具有高稳定性和光催化活性的基于 $CsPbX_3$ 的异质结构提供了有效的策略。

关 键 词: 钙钛矿量子点; 二维超薄纳米片; 光催化; $CsPbBr_3$; g-C_3N_4

中图分类号: O649 **文献标志码**: A